Confinement of Relativistic Electrons in a Magnetic Mirror en Route to a Magnetized Relativistic Pair Plasma

J. von der Linden, G. Fiksel, J. Peebles, M. Edwards, L. Willingale, A. Link, D. Mastrosimone, H. Chen

May 17, 2021

Physics of Plasmas

Confinement of Relativistic Electrons in a Magnetic Mirror en Route to a Magnetized Relativistic Pair Plasma

J. von der Linden,[1, a)] G. Fiksel,[2] J. Peebles,[3] M. R. Edwards,[1] L. Willingale,[2] T. Link,[1]
D. Mastrosimone,[3] and H. Chen[1]

[1)] *Lawrence Livermore National Laboratory, Livermore, CA 94550, USA*
[2)] *Center for Ultrafast Optical Science, University of Michigan, Ann Arbor, MI 48109, USA*
[3)] *Laboratory for Laser Energetics, University of Rochester, Rochester, NY 14623, USA*

(Dated: 6 April 2021)

Creating magnetized relativistic pair plasma in the laboratory would enable the exploration of unique plasma physics relevant to some of the most energetic events in the universe. As a step towards a laboratory pair plasma, we have demonstrated effective confinement of multi-MeV electrons inside a pulsed-power-driven 13 T magnetic mirror field with a mirror ratio of 2.6. The confinement is diagnosed by measuring the axial and radial losses with magnetic spectrometers. The loss spectra are consistent with ≤ 2.5 MeV electrons confined in the mirror with confinement time of ~ 1 ns. With a source of 10^{12} electron-positron pairs at comparable energies, this magnetic mirror would confine a relativistic pair plasma with Lorentz factor $\gamma \sim 6$ and magnetization $\sigma \sim 40$.

[a)] Electronic mail: jens.von.der.linden@ipp.mpg.de; Current address: Division E4, Max Planck Institute for Plasma Physics, 17491 Greifswald and 85748 Garching, Germany

I. INTRODUCTION

Pair plasma of positrons and electrons behave drastically different from ion-electron plasmas due to their unity mass ratio[1]. The unity mass ratio alters the waves[2] and unstable modes[3] in a pair plasma. In addition, due to their lower mass electron-positron plasma can achieve relativistic and magnetized conditions relevant to energetic astrophysical phenomena with $1/1000$ of the kinetic energy and $1/30$ of the magnetic field of electron-proton plasmas.

Relativistic plasmas are found in energetic astrophysical systems abundant in antimatter, such as supernova remnants, gamma-ray bursts, and active galactic nuclei[4,5]. The jets of active galatic nuclei[6] as well as the magnetospheres of pulsars[7] contain magnetically dominated plasma where particles may be energized through relativistic magnetic reconnection[8] and kink instabilities[9]. In all these systems intense non-thermal radiation is thought to result from collisionless shocks formed by magnetic field amplification or generation in Weibel-like instabilities[10]. These Weibel-like instabilities are electromagnetic instabilities in plasmas with momentum anistropy[11]. Electromagnetic instabilities generally dominate over electrostatic modes (e.g. the two-stream instability) when the plasma has relativistic energies[12]. Which electromagnetic instability dominates the mode spectrum has been the subject of recent theoretical work investigating the effects of ratio of thermal to directed momentum[13], magnetization[14] and mass ratios[12]. The unity mass ratio of electron-positron plasma is predicted to lead to 100x faster growth rates than in electron-proton plasma[12].

Although laboratory positron-electron plasma reduce the particle energy and magnetic field needed to achieve these relativistic and magnetically dominated regimes, the difficulty in producing a large number of positrons and in containing them for long lifetimes has so far precluded their use. In recent decades much progress has been made in producing reliable positron sources. Positrons with energies of tens to hundreds of eV can be harnessed with continuous fluxes of 10^9 s^{-1} through capture of fission neutrons and moderation[15] and in μs pulses of 1.5×10^5 with 40 Hz repetition rates through electron-target interactions and moderation at radio frequency accelerator facilities[16]. Short pulse ($\sim$ 10 ps) laser-target interactions generate large numbers of multi-MeV positrons[17], up to a 10^{12}. This favors laser-matter interactions as source for relativistic pair plasma experiments[5].

A plasma is relativistic when the Lorentz factor $\gamma > 2$, i.e. the kinetic energy of particles exceeds their rest mass, 511 KeV for electrons and positrons. To study electromagnetic instabilities with these relativistic pairs it is necessary for the plasma to be dense enough to attenuate electromagnetic waves. This means that the scale length of the plasma must be larger than the skin depth $\lambda_s = c/\sqrt{ne^2/(\varepsilon_0 \gamma m_e)}$, c is the speed of light, n is the number density of electrons *and* positrons as both respond quickly to perturbations[2], e the elementary charge, m_e the electron (and positron) mass, and ε_0 the permittivity of free space. In addition, the lifetime of the plasma needs to be greater than the instability growth rate τ, which is related to the inverse of the plasma frequency ($\tau \propto 1/\omega_p$)[17]. This can be achieved in either beams of pairs dense enough to result in instability growth during the time of flight[18,19] or in less dense magnetically confined pairs.

Here, we focus on developing magnetic traps in order to study magnetized and relativistic pair plasma[5]. A (relativistic) pair plasma is considered magnetically dominated when the magnetization factor - the ratio of magnetic energy density over particle energy density $\sigma = (B^2/\mu_0)/(n\gamma m_e c^2)$ - exceeds unity, where B is the magnetic field, μ_0 the permeability of free space, and c the speed of light. Magnetic configurations can trap pairs with magnetic mirroring effects. This has been successfully demonstrated with lower-energy positrons: a magnetic mirror[20] trapped eV positrons for > 70 ms, the magnetic dipole field of a permanent magnet[21] has trapped eV positrons for > 1 s, and the dipole field of a levitating superconductor[22] has trapped 100 KeV positrons for 100 μs. Here, we report on the design of a magnetic mirror for confinement of laser-generated MeV pairs in a cm-sized mirror and demonstrate its confinement properties by injecting laser-target generated relativistic electrons.

II. MIRROR DESIGN

Inhomogenous magnetic fields exert a force on pairs opposite to the field gradient[23], $F = -\mu \nabla B$, where $\mu = \gamma m_e u_\perp^2/(2B)$ is the magnetic moment of the particle with perpendicular velocity $u_\perp$. A magnetic mirror traps charged particles between two maxima of the magnetic field. The trapped particles complete three motions in a magnetic mirror: they gyrate around the magnetic field lines, they bounce back and forth between the maxima and they drift azimuthally around the mirror axis[5]. Each of these motions is associated with an adiabatic invariant which is conserved if the magnetic field varies slowly spatial and temporally over a cycle of the motion. The invariants can be derived from action integrals of the canonical momentum associated with the three motions: gyration perpendicular to the field $P_\perp$, bounce parallel to the field $P_\parallel$, and drift in the azimuthal direction P_θ along the respective path dl[24]. The relativistic adiabatic invariant of the

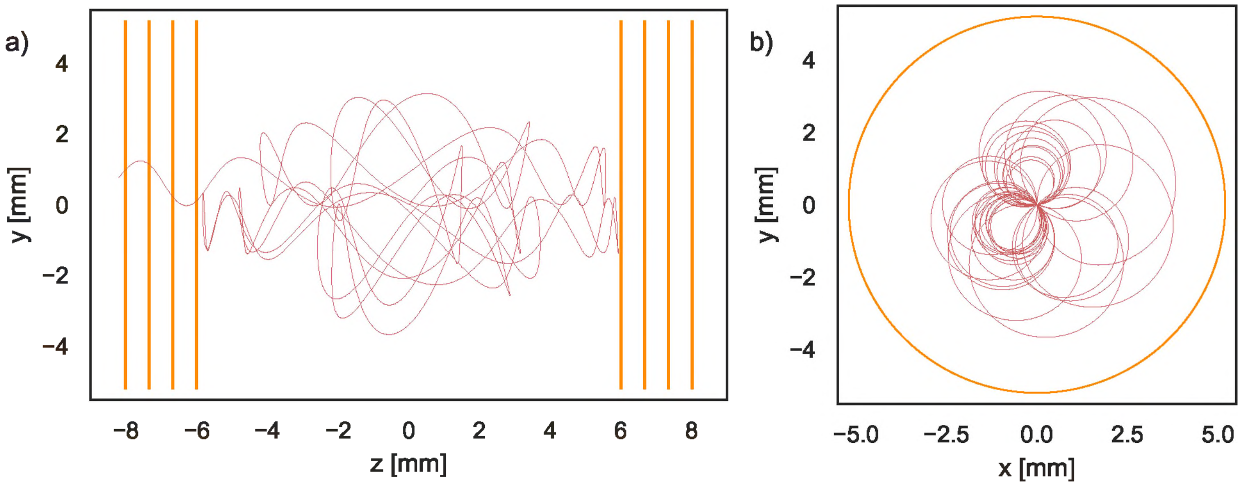

FIG. 1. Numerically integrated path of a 2.5 MeV electron launched with pitch angle 51° from the mirror center. The electron is lost after 0.92 ns. a) View perpendicular to mirror axis shows gyro and bounce motion. b) View along mirror axis shows drift.

gyromotion M_r differs from the magnetic moment used to calculate the mirror force by an additional factor of gamma, $M_r = \int P_\perp dl = \gamma\mu$. The longitudinal invariant J constrains the bounce motion $u_{||}$, $J = \int P_{||} dl = \gamma u_{||} dl$. The azimuthal magnetic vector potential A_θ dominates the electron momentum $\gamma m_e u_\theta$ in the azimuthal canonical momentum so that the third invariant reduces to the magnetic flux enclosed by the drift motion $\phi = \int P_\theta dl = \int (qA_\theta + \gamma m_e u_\theta) dl \sim \int \vec{B} \cdot dS$. To conserve the first two adiabatic invariants the Larmor radius $r_L = \gamma m u_\perp / (qB)$ of particles needs to be much smaller than the scale length of the magnetic field. For a simple magnetic mirror generated by two solenoids the scale length can be approximated as the solenoid radius. Yet, conservation of all adiabatic invariants is not a necessary condition to trap particles for several bounce periods[22]. For example, keeping the Larmor radius of 2.5 MeV electrons and positrons a factor of 10 shorter than a coil radius of 0.5 cm would require a 20 T field in the center of the mirror. Integrating the relativistic equation of motion, $d/dt(\gamma m_e \vec{u}) = q\vec{u} \times \vec{B}$, reveals that a 2.5 MeV electron is trapped in a mirror field with 5 T in the mirror center and 13 T in the coil centers for several bounce periods with a chaotic path (fig. 1 a). Despite the chaotic path the drift is still axis encircling, tracing a circular surface of constant flux (fig. 1 b). As the mirror field is axisymmetric angular canonical momentum of charged particles and correspondingly the magnetic flux their drifts enclose is conserved even over strongly varying fields[25].

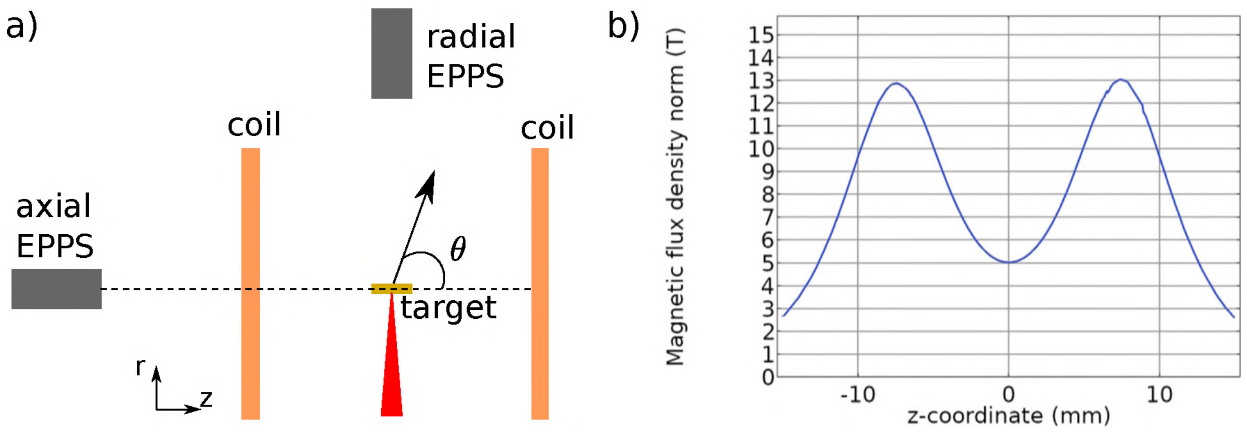

FIG. 2. a) Laser-target interaction generates electrons in mirror field generated by two MIFEDS coils (orange). Target (gold) is centered between coils. Two EPPS magnetic spectrometers measure axial and radial losses. The electron divergence is characterized by the polar angle θ with respect to the mirror axis (dashed). b) Magnetic field along mirror axis. $z = 0$ is the mirror center.

The magneto-inertial fusion discharge system (MIFEDS)[26–29] at the Omega EP short pulse laser facility can store $\sim$ 500 J. This is enough to produce the magnetic field as used in the particle tracing in fig. 1 between two 10 mm coils spaced 14 mm apart with a 28 kA current pulse lasting μs. The mirror MIFEDS coil can be arranged so that the mirror is centered at target chamber center where a target is placed to generate pairs through laser-matter interaction. The trapping of electrons and positrons in this mirror will depend on the pitch angles of perpendicular velocity to parallel velocity the particles are injected into the mirror. A previous characterization[30] of electrons and positrons leaving a 1-mm Au target have found angular distributions with full widths at half maximum (FWHM) of $50^\circ \pm 10^\circ$. The divergence can be characterized in terms of the polar angle θ with respect to the mirror axis (fig. 2). If a target were placed in the center of the mirror with the target normal perpendicular to the mirror axis, the angular distribution of particles would be centered along the target normal, at 90° to the mirror axis.

To evaluate the confinement properties the MIFEDS mirror we numerically integrate the paths of 100 electrons with 2.5 MeV kinetic energy launched with this angular divergence from the center of the mirror. Fig. 3 shows the time evolution of the number of 2.5 MeV electrons in the 13 MeV mirror (blue). The e-folding time of the number of confined electrons is $\sim$ 2 ns. The losses are due to axial outflows of electrons, including from initially trapped electrons that move non-adiabatically into the loss cone. As the mirror is a closed system the phase space of electrons

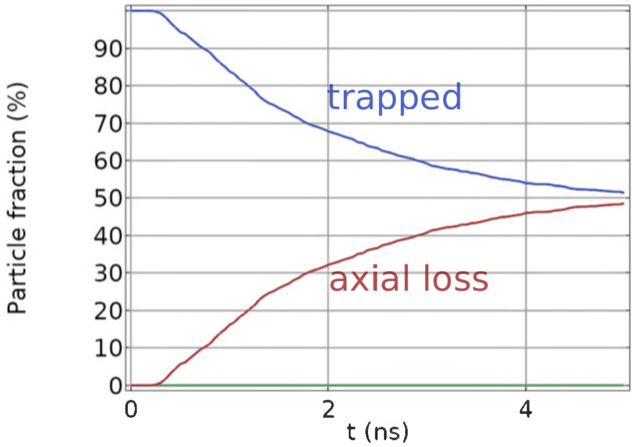

FIG. 3. Trapped 2.5 MeV electrons (blue) in the 13 T magnetic mirror. The trapping time is limited by axial outflows (red).

can be described with Liouville's theorem and all trapped electron paths, even chaotic ones, will eventually cross their origin, the target. Collisions with the target scatter the electrons, perhaps shifting their pitch angle into the loss cone. Even with the pessimistic assumption that all target collisions are losses, for a 20 μm thick and 0.5 mm electrons are still trapped for several bounces with e-folding time of 1 ns.

We can diagnose losses from the mirror with magnetic spectrometers placed outside the mirror. Fig. 4 shows the trajectories of 2, 3, 5, and 13 MeV electrons in the mirror, without any collective effects. 2 MeV electrons are only lost axially and only for shallow launching angles with respect to the mirror axis, while at higher energies electrons are also lost radially. At higher energies an increasing portion of electrons is not trapped at all. Instead they exit the mirror in less than one gyro-orbit. The trajectories of 3, 5 and 13 MeV electrons exhibit non-axisymmetry, as the electrons sweep a radial loss angle corresponding to the portion of the gyro-orbit they complete before leaving the mirror field. There is also a gap in losses at polar angles intersecting the coils. That is, an electron cannot escape by penetrating the coil due to a strong field near the wire surface. Two orthogonal magnetic electron-positron-proton spectrometers (EPPS)[31] can validate these calculated loss spectra. Ratios of the flux ψ of simulated electrons launching from the target with no magnetic field applied and the magnetic field applied $\psi(B = 13\text{ T})/\psi(B = 0\text{ T})$ quantify the effect of the magnetic mirror without requiring knowledge of the angular dependence of the electron number (fig.5). The magnetic field increases the number of ≤ 2.5 MeV electrons exiting the mirror radially (ratio < 1) and corresponding increases the number exiting axially (ratio > 1).

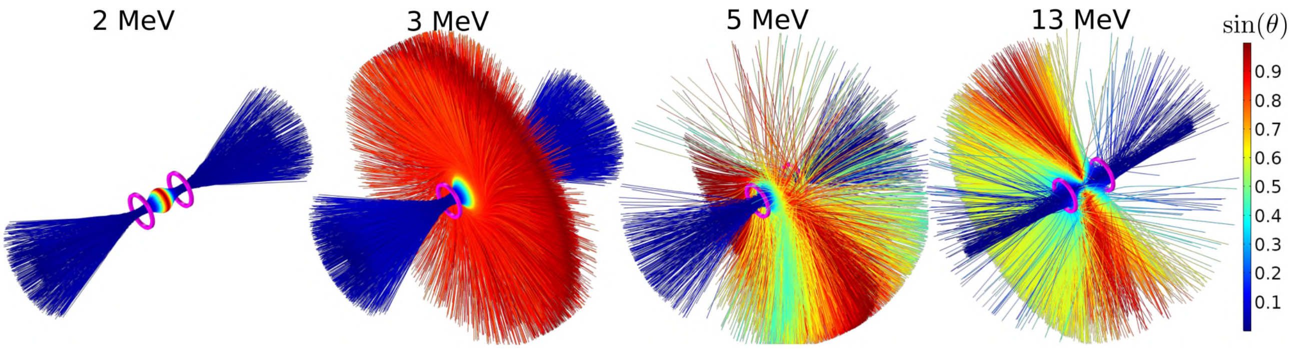

FIG. 4. Trajectories of 2, 3, 5, 13 MeV electrons exiting magnetic mirror formed by two 13 T coils (coils shown in pink). 2 MeV electrons are only lost axially and only for shallow launching angles with respect to the mirror axis, while at higher energies electrons are also lost radially. 3 MeV, 5 MeV, and 13 MeV radial electron losses are non-axisymmetric, the electrons sweep a radial loss angle with increasing energy. The color of the trajectories corresponds to sin(θ), where θ is the polar angle with respect to the mirror axis at which the electron is launched.

At higher energies the effect of the magnetic field becomes negligible (ratio $\sim$ 1); however, the ratios do not very monotonically with energy.

III. EXPERIMENT SETUP

We conduct experiments at Omega EP to demonstrate the confinement properties of the high field mirror for relativistic electrons. The target dimensions, 20 μs thick and 0.5 mm, are optimized for electron production the short 20 μm thickness of the target limits the production of positrons through the Bethe-Heitler process[32] to levels just above the noise floor. The relativistic electrons are generated by interaction of an Omega EP 10 ps pulse[33] with wavelength $\lambda = 1054$ nm with the target. A background shot is taken with no applied magnetic field. The magnetic mirror field is applied for five shots; three with 13 T and two with 9 T at the coil center. The laser energies is 900 ± 20 J, corresponding to an intensity in the first two shots. However, after the first magnetized shot MIFEDS debris and copper disposition on the laser optics reduces the laser energy to 770 ± 40 J. With 80% of the laser energy contained within a 16 ± 2 μm radius the laser energies correspond to intensities of $I = 9 \pm 1 \times 10^{18}$ W/cm^2 and $I = 7 \pm 1 \times 10^{18}$ W/cm^2, respectively. The laser power contrast is about $10^8 - 10^9$. At such laser conditions, the radially escaping spectrum (fig. 6) fits a Maxwellian-like exponential with temperature $T = 5.8 \pm 1$ MeV, close to the expected

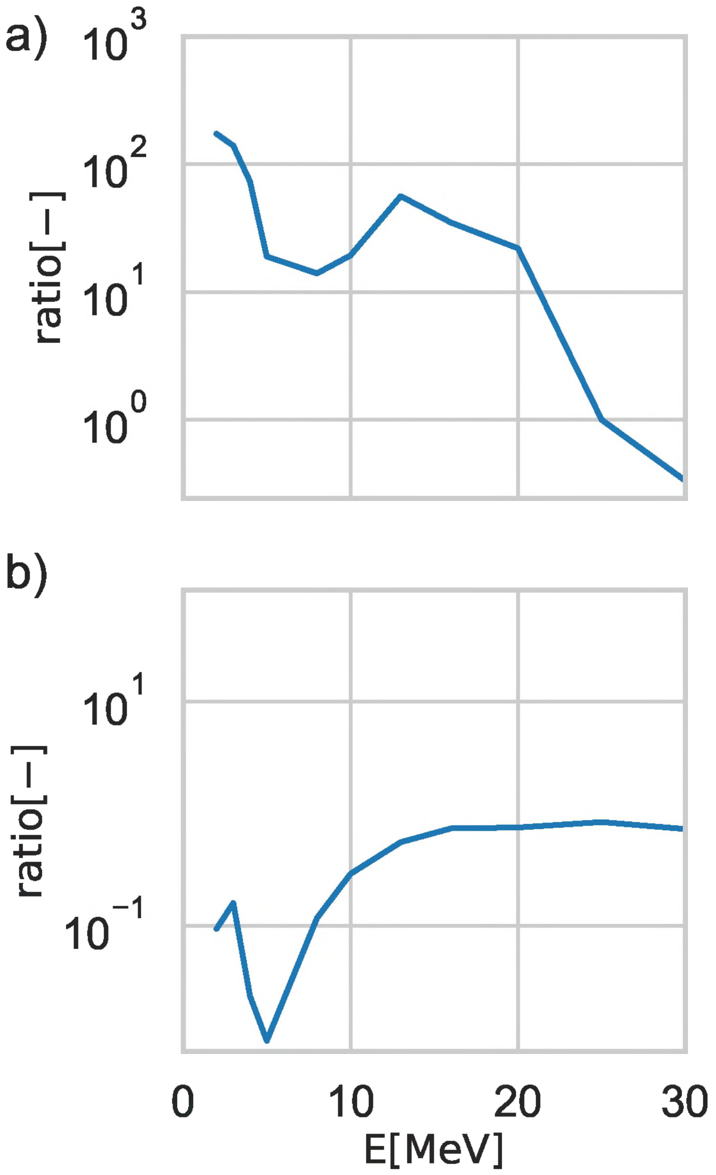

FIG. 5. Ratio of $B = 13$ T to $B = 0$ T simulated a) axial and b) radial electron loss fluxes.

value according to Pukhov scaling[34], 4.7 MeV, and within previous measured range[35] for the unmagnetized shot laser intensity $9 \cdot 10^{18}$.

IV. RESULTS & ANALYSIS

Two electron-positron-proton spectrometers (EPPS) are positioned to sample the electron losses placed parallel to the MIFEDS magnetic mirror axis and normal to the mirror axis, radial with respect to the mirror geometry (fig. 2). Each EPPS accepts particles through a 0.95×0.96 mm^2

slit. The radial EPPS is 48 cm and the axial EPPS is 57 cm from the center of the mirror which is also the target chamber center. After each shot the image plates from the two EPPS are scanned after 25 minutes and adjusted for fading with a factor of 0.67 as derived from Tanaka et al.[36]. Two super-Gaussians are fitted to the background and signal on each image plate in order to remove the background and determine the projected slit width[37]. Calibrations of the absolute dose[38] and dispersion with measurements in the expected trapped particle energies[39], $3-15$ MeV, provide absolute electron energy spectra. Without the magnetic field the electrons exit mostly radially, normal to the target surface. The electron energy distribution is determined by the laser-plasma acceleration processes in the preformed plasma on the surface of the target[40,41]. Refluxing of electrons in the target may broaden the energy distribution. The axial loss spectrum corresponds to the angular divergence of electrons leaving the target. In shots with applied magnetic field the radial electron loss spectra have three characteristic differences to the baseline no-magnetic-field shot (fig. 6): 1) the radial EPPS measures a significantly lower number of electrons, 2) the energy spectrum has a steep drop at 3.7 MeV, 3) followed by a steady increase until 14 MeV (18 MeV) for the 9 T (13 T) field. The energy spectrum of axial losses is shifted upward in shots with a magnetic field and there are several narrow spikes with energies below 5 MeV followed by a broad spike at 10 MeV (13 MeV) for 9 T (13 T). The spikes in the axial electron spectra can be explained by magnetic lensing effects[42]. Each solenoid acts as a lens for charged particles with a focal length f that can be approximated by $f \sim 3.4\rho_{ce}^2/a$, where $\rho_{ce} = \gamma m_e u/(q_e B_0)$ is the electron gyroradius where B_0 the magnetic field at the coil center, q_e is the charge with sign, and a the coil diameter. The energy of the broad peaks in the axial spectrum corresponds to the electron energy for which the focal length is the coil-to-target distance 7.5 mm, i.e. the energy of electrons that should be collimated[43]. The thin spikes have been noted in magnetic focusing experiments[32] and correspond to complicated trajectories of specific energy electrons which focus and subsequently re-collimate upon exiting the coil. To relate the measured losses to the calculated particle trajectories we compare the numerical electron flux $\psi(B = 13\text{ T})/\psi(B = 0\text{ T})$ from the calculated trajectories to the ratios of the measured spectra (fig.7). The simulated flux ratios are consistent with the characteristics observed in the measured fluxes: 1) the radial flux is significantly reduced and the axial flux is correspondingly enhanced, 2) the radial flux sharply drops off for energies above 3.7 MeV and 3) followed by a steady increase until 18 MeV for the 13 T. The reduction in the radially lost electrons and corresponding increase in axially lost electrons agrees with the path integrations of trapped electrons lost along the axial loss cones. The drop and steady increase are

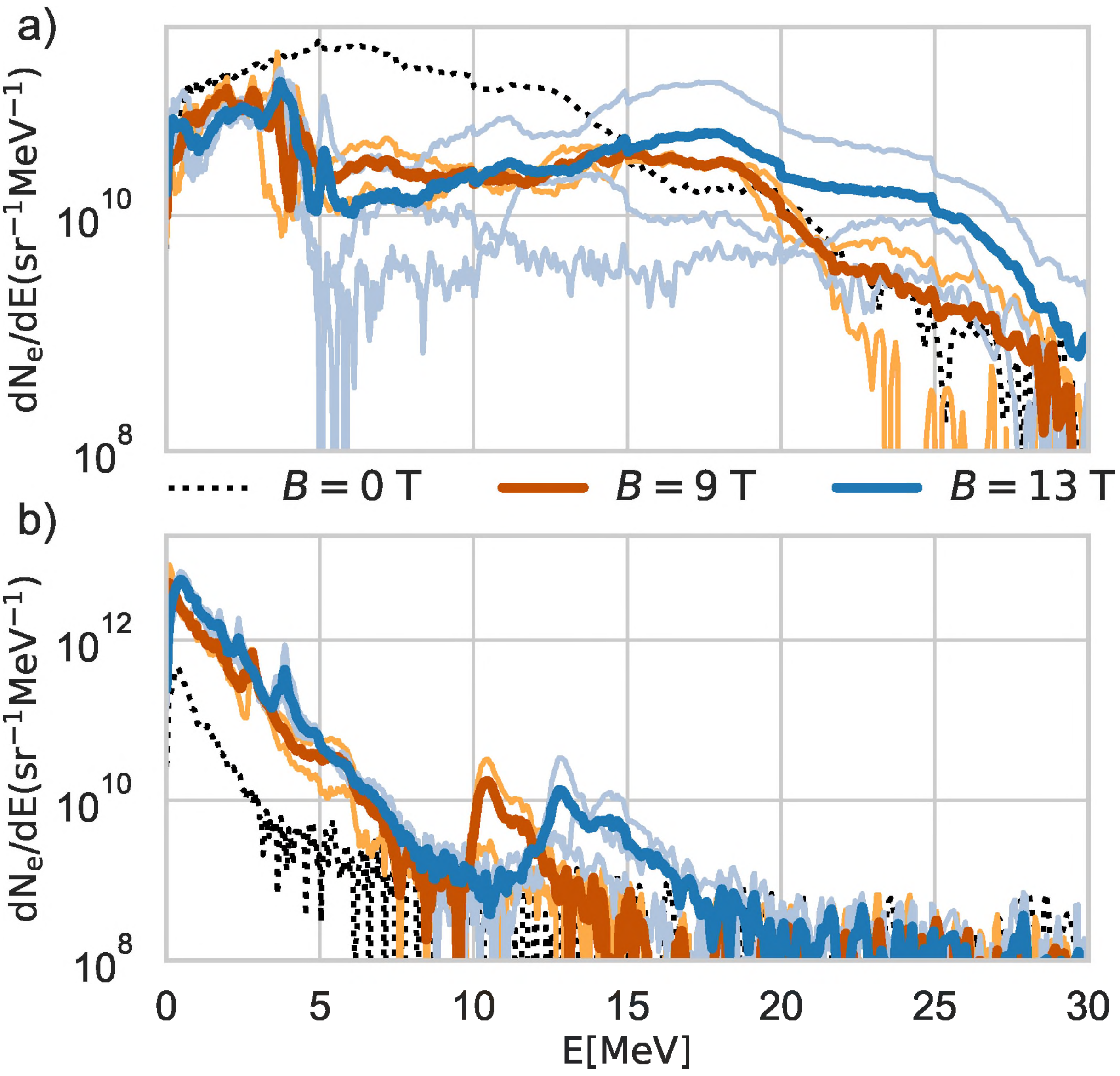

FIG. 6. EPPS measured spectra of escaping electrons. Spectra of a) radially and b) axially escaping electrons with no magnetic field (dashed back), 3 shots with 13 T magnetic field at the coil centers (light blue; average of shots thick blue), and 2 shots with 9 T magnetic field at coil centers (light orange; average of shots thick dark orange).

due to electrons completing only one or even less than one gyro-orbit before leaving the magnetic mirror and are at first deflected away from the radial EPPS and as their energy increases they are deflected less.

As the mirror force is independent of the sign of the charge, this mirror should be able to confine

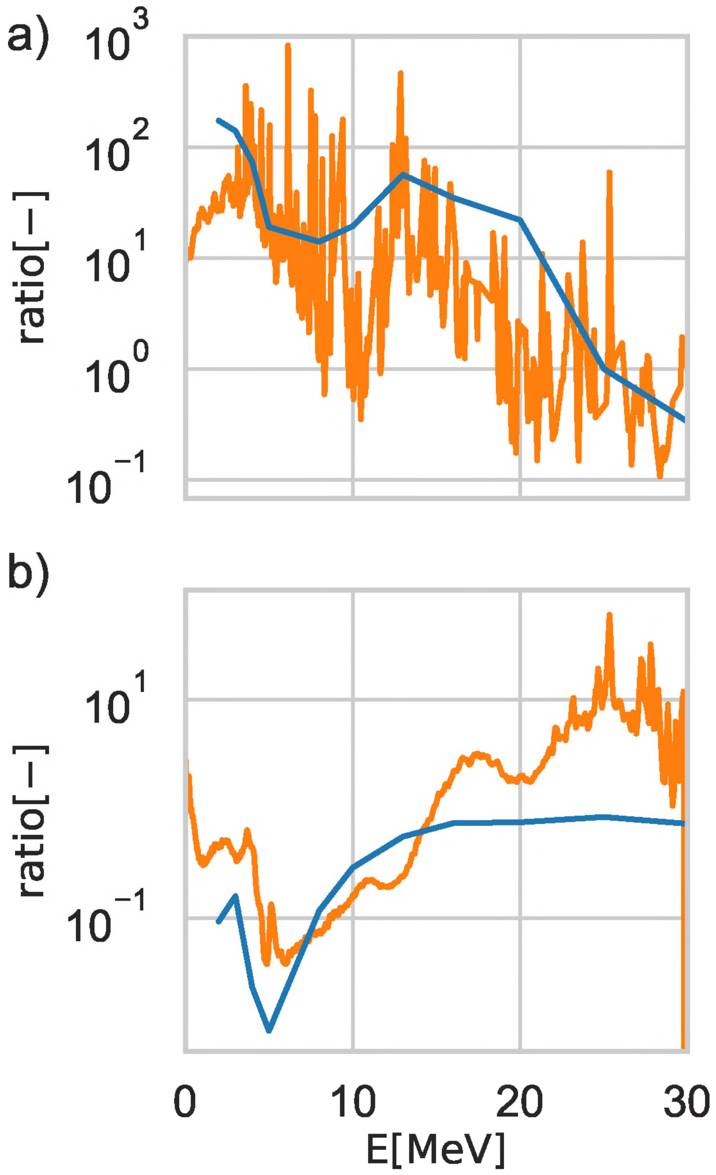

FIG. 7. Ratio of $B = 13$ T to $B = 0$ T simulated a) axial and b) radial electron loss fluxes (blue) plotted together with respective ratio of measured loss spectra (orange).

positrons and electrons simultaneously. Positrons and electrons could be generated outside of the mirror with thicker targets optimized for positron production. The pairs could then be magnetically transported to the mirror with a solenoid acting as collimating lens. The lens would select particle energy and if tilted select charge[43] so that a unity charge ratio pair beam could be injected into the mirror. A thin foil placed inside the mirror could scatter the injected pairs out of the loss cone[5]. The coils could also be arranged in a cusp configuration with a magnetic null at the center, this may simplify injection from an outside target as the magnetic null would allow pairs to transition non-adiabatically to trapped particles[44].

V. CONCLUSION

Measurements of the axial and radial losses from the magnetic mirror are consistent with numerically calculated electron losses and confinement of ≤ 2.5 MeV. This 13 T magnetic mirror formed by two pulsed power coils can trap relativistic electrons and/or positrons for nanoseconds. The largest positron yield achieved with intense laser-matter interaction[17] is 10^{12}. In the mirror discussed here that would correspond to a density of 10^{12} cm^{-3} which with Debye length and skin depth on the order of the mirror would approach the plasma conditions for supporting electrostatic and electromagnetic instabilities[5]. The pairs would be relativistic with $\gamma \sim 6$ and magnetized with $\sigma \sim 40$. Increases in the magnetic field could increase the energy of pairs that can be trapped. For example, the upgrade of the pulsed power supply at OMEGA from MIFEDS-2 to MIFEDS-3 will increase the stored electric energy from 200 J to 2 kJ, enabling higher currents and corresponding magnetic fields to be driven in the coils[28].

ACKNOWLEDGMENTS

We gratefully acknowledge the support of the Omega EP facility during these Laboratory Basic Science experiments and helpful discussions about adiabatic invariants for relativistic trapped particles with Eve V. Stenson, Stefan Nissl, and Matthew R. Stoneking. This work was performed under the auspices of the U.S. Department of Energy by Lawrence Livermore National Laboratory under Contract DE-AC52-07NA27344 and was supported by the LLNL-LDRD Program under Project No. 20-LW-021. LLNL-JRNL-XXXXXX.

Security, LLC. The views and opinions of authors expressed herein do not necessarily state or reflect those of the United States government or Lawrence Livermore National Security, LLC, and shall not be used for advertising or product endorsement purposes.

DATA AVAILABILITY

The data that support the findings of this study are available from the corresponding author upon reasonable request.

REFERENCES

[1] V. Tsytovich and C. B. Wharton, "Laboratory electron-positron plasma - a new research object," Comments on Plasma Physics and Controlled Fusion **4**, 91–100 (1978).

[2] E. V. Stenson, J. Horn-Stanja, M. R. Stoneking, and T. S. Pedersen, "Debye length and plasma skin depth: two length scales of interest in the creation and diagnosis of laboratory pair plasmas," Journal of Plasma Physics **83** (2017).

[3] A. Bret, A. S. Novo, R. Narayan, C. Ruyer, M. E. Dieckmann, and L. O. Silva, "Theory of the formation of a collisionless weibel shock: pair vs. electron/proton plasmas," Laser and Particle Beams **34**, 362–367 (2016).

[4] H.-S. Park, D. Ryutov, J. Ross, N. Kugland, S. Glenzer, C. Plechaty, S. Pollaine, B. Remington, A. Spitkovsky, L. Gargate, G. Gregori, A. Bell, C. Murphy, Y. Sakawa, Y. Kuramitsu, T. Morita, H. Takabe, D. Froula, G. Fiksel, F. Miniati, M. Koenig, A. Ravasio, A. Pelka, E. Liang, N. Woolsey, C. Kuranz, R. Drake, and M. Grosskopf, "Studying astrophysical collisionless shocks with counterstreaming plasmas from high power lasers," High Energy Density Physics **8**, 38–45 (2012).

[5] M. R. Stoneking, T. S. Pedersen, P. Helander, H. Chen, U. Hergenhahn, E. V. Stenson, G. Fiksel, J. von der Linden, H. Saitoh, C. M. Surko, J. R. Danielson, C. Hugenschmidt, J. Horn-Stanja, A. Mishchenko, D. Kennedy, A. Dellar, A. Card, S. Nißl, M. Singer, M. Singer, S. König, L. Willingale, J. Peebles, M. R. Edwards, and K. Chin, "A new frontier in laboratory physics: magnetized electron–positron plasmas," Journal of Plasma Physics **86**, 155860601 (2020).

[6] T. di Matteo, "Magnetic reconnection: flares and coronal heating in active galactic nuclei," Monthly Notices of the Royal Astronomical Society **299**, L15–L20 (1998).

[7] Y. Lyubarsky and J. G. Kirk, "Reconnection in a striped pulsar wind," The Astrophysical Journal **547**, 437–448 (2001).

[8] Y. E. Lyubarsky, "On the relativistic magnetic reconnection," Monthly Notices of the Royal Astronomical Society **358**, 113–119 (2005).

[9] O. Bromberg and A. Tchekhovskoy, "Relativistic MHD simulations of core-collapse GRB jets: 3D instabilities and magnetic dissipation," Monthly Notices of the Royal Astronomical Society **456**, 1739–1760 (2015).

[10] T.-Y. B. Yang, Y. Gallant, J. Arons, and A. B. Langdon, "Weibel instability in relativistically hot magnetized electron–positron plasmas," Physics of Fluids B: Plasma Physics **5**, 3369–3387 (1993).

[11] E. S. Weibel, "Spontaneously growing transverse waves in a plasma due to an anisotropic velocity distribution," Physical Review Letters **2**, 83–84 (1959).

[12] A. Bret, A. Stockem, F. Fiuza, C. Ruyer, L. Gremillet, R. Narayan, and L. O. Silva, "Collisionless shock formation, spontaneous electromagnetic fluctuations, and streaming instabilities," Physics of Plasmas **20**, 042102 (2013).

[13] A. Stockem, F. Fiuza, A. Bret, R. A. Fonseca, and L. O. Silva, "Exploring the nature of collisionless shocks under laboratory conditions," Scientific Reports **4** (2014), 10.1038/srep03934.

[14] A. Bret, "Hierarchy of instabilities for two counter-streaming magnetized pair beams," Physics of Plasmas **23**, 062122 (2016).

[15] C. Hugenschmidt, C. Piochacz, M. Reiner, and K. Schreckenbach, "The NEPOMUC upgrade and advanced positron beam experiments," New Journal of Physics **14**, 055027 (2012).

[16] H. Higaki, K. Michishio, K. Hashidate, A. Ishida, and N. Oshima, "Accumulation of LINAC based low energy positrons in a buffer gas trap," Applied Physics Express **13**, 066003 (2020).

[17] H. Chen, F. Fiuza, A. Link, A. Hazi, M. Hill, D. Hoarty, S. James, S. Kerr, D. Meyerhofer, J. Myatt, J. Park, Y. Sentoku, and G. Williams, "Scaling the yield of laser-driven electron-positron jets to laboratory astrophysical applications," Physical Review Letters **114** (2015).

[18] E. Liang, T. Clarke, A. Henderson, W. Fu, W. Lo, D. Taylor, P. Chaguine, S. Zhou, Y. Hua, X. Cen, X. Wang, J. Kao, H. Hasson, G. Dyer, K. Serratto, N. Riley, M. Donovan, and T. Ditmire, "High e+/e- ratio dense pair creation with 10^{21} w.cm-2 laser irradiating solid targets," Scientific Reports **5** (2015), 10.1038/srep13968.

[19] G. Sarri, K. Poder, J. M. Cole, W. Schumaker, A. D. Piazza, B. Reville, T. Dzelzainis, D. Doria, L. A. Gizzi, G. Grittani, S. Kar, C. H. Keitel, K. Krushelnick, S. Kuschel, S. P. D. Mangles,

Z. Najmudin, N. Shukla, L. O. Silva, D. Symes, A. G. R. Thomas, M. Vargas, J. Vieira, and M. Zepf, "Generation of neutral and high-density electron–positron pair plasmas in the laboratory," Nature Communications **6** (2015), 10.1038/ncomms7747.

[20]H. Higaki, C. Kaga, K. Fukushima, H. Okamoto, Y. Nagata, Y. Kanai, and Y. Yamazaki, "Simultaneous confinement of low-energy electrons and positrons in a compact magnetic mirror trap," New Journal of Physics **19**, 023016 (2017).

[21]J. Horn-Stanja, S. Nißl, U. Hergenhahn, T. S. Pedersen, H. Saitoh, E. Stenson, M. Dickmann, C. Hugenschmidt, M. Singer, M. Stoneking, and J. Danielson, "Confinement of positrons exceeding 1 s in a supported magnetic dipole trap," Physical Review Letters **121** (2018), 10.1103/physrevlett.121.235003.

[22]H. Saitoh, Z. Yoshida, Y. Yano, M. Nishiura, Y. Kawazura, J. Horn-Stanja, and T. S. Pedersen, "Chaos of energetic positron orbits in a dipole magnetic field and its potential application to a new injection scheme," Physical Review E **94** (2016).

[23]D. R. Nicholson, *Introduction to Plasma Theory* (Wiley & Sons, New York, 1983).

[24]T. G. Northrop, "Adiabatic charged-particle motion," Reviews of Geophysics **1**, 283 (1963).

[25]P. M. Bellan, *Fundamentals of Plasma Physics* (Cambridge University Press, 2004).

[26]G. Fiksel, R. Backhus, D. H. Barnak, P.-Y. Chang, J. R. Davies, D. Jacobs-Perkins, P. McNally, R. B. Spielman, E. Viges, and R. Betti, "Inductively coupled 30 T magnetic field platform for magnetized high-energy-density plasma studies," Review of Scientific Instruments **89**, 084703 (2018).

[27]D. H. Barnak, J. R. Davies, G. Fiksel, P.-Y. Chang, E. Zabir, and R. Betti, "Increasing the magnetic-field capability of the magneto-inertial fusion electrical discharge system using an inductively coupled coil," Review of Scientific Instruments **89**, 033501 (2018).

[28]R. Shapovalov, G. Brent, R. Moshier, M. Shoup, R. Spielman, and P.-A. Gourdain, "Design of 30-T pulsed magnetic field generator for magnetized high-energy-density plasma experiments," Physical Review Accelerators and Beams **22** (2019), 10.1103/physrevaccelbeams.22.080401.

[29]J. Peebles, "Current Capabilities of the MIFEDS System," Meeting on Magnetic Fields in Laser Plasmas (2018).

[30]H. Chen, S. C. Wilks, D. D. Meyerhofer, J. Bonlie, C. D. Chen, S. N. Chen, C. Courtois, L. Elberson, G. Gregori, W. Kruer, O. Landoas, J. Mithen, J. Myatt, C. D. Murphy, P. Nilson, D. Price, M. Schneider, R. Shepherd, C. Stoeckl, M. Tabak, R. Tommasini, and P. Beiersdorfer, "Relativistic quasimonoenergetic positron jets from intense laser-solid interactions," Physical Review

Letters **105** (2010), 10.1103/physrevlett.105.015003.

[31] H. Chen, A. J. Link, R. van Maren, P. K. Patel, R. Shepherd, S. C. Wilks, and P. Beiersdorfer, "High performance compact magnetic spectrometers for energetic ion and electron measurement in ultraintense short pulse laser solid interactions," Review of Scientific Instruments **79**, 10E533 (2008).

[32] G. J. Williams, D. Barnak, G. Fiksel, A. Hazi, S. Kerr, C. Krauland, A. Link, M. J.-E. Manuel, S. R. Nagel, J. Park, J. Peebles, B. B. Pollock, F. N. Beg, R. Betti, and H. Chen, "Target material dependence of positron generation from high intensity laser-matter interactions," Physics of Plasmas **23**, 123109 (2016).

[33] L. Waxer, D. Maywar, J. Kelly, T. Kessler, B. Kruschwitz, S. Loucks, R. McCrory, D. Meyerhofer, S. Morse, C. Stoeckl, and J. Zuegel, "High-energy petawatt capability for the omega laser," Optics and Photonics News **16**, 30 (2005).

[34] A. Pukhov, Z.-M. Sheng, and J. Meyer-ter-Vehn, "Particle acceleration in relativistic laser channels," Physics of Plasmas **6**, 2847–2854 (1999).

[35] H. Chen, A. Link, Y. Sentoku, P. Audebert, F. Fiuza, A. Hazi, R. F. Heeter, M. Hill, L. Hobbs, A. J. Kemp, G. E. Kemp, S. Kerr, D. D. Meyerhofer, J. Myatt, S. R. Nagel, J. Park, R. Tommasini, and G. J. Williams, "The scaling of electron and positron generation in intense laser-solid interactions," Physics of Plasmas **22**, 056705 (2015).

[36] K. A. Tanaka, T. Yabuuchi, T. Sato, R. Kodama, Y. Kitagawa, T. Takahashi, T. Ikeda, Y. Honda, and S. Okuda, "Calibration of imaging plate for high energy electron spectrometer," Review of Scientific Instruments **76**, 013507 (2005).

[37] J. Park, *The effects of preformed plasmas on the directionality of the relativistic electron beam*, Ph.D. thesis, University of California (2015).

[38] H. Chen, N. L. Back, T. Bartal, F. N. Beg, D. C. Eder, A. J. Link, A. G. MacPhee, Y. Ping, P. M. Song, A. Throop, and L. Van Woerkom, "Absolute calibration of image plates for electrons at energy between 100 KeV and 4 MeV," Review of Scientific Instruments **79**, 033301 (2008).

[39] J. von der Linden, J. Ramos-Méndez, B. Faddegon, D. Massin, G. Fiksel, J. P. Holder, L. Willingale, J. Peebles, M. R. Edwards, and H. Chen, "Dispersion calibration for the National Ignition Facility electron–positron–proton spectrometers for intense laser matter interactions," Review of Scientific Instruments **92**, 033516 (2021).

[40] S. C. Wilks, W. L. Kruer, M. Tabak, and A. B. Langdon, "Absorption of ultra-intense laser pulses," Physical Review Letters **69**, 1383–1386 (1992).

[41] A. Kemp, F. Fiuza, A. Debayle, T. Johzaki, W. Mori, P. Patel, Y. Sentoku, and L. Silva, "Laser–plasma interactions for fast ignition," Nuclear Fusion **54**, 054002 (2014).

[42] H. Chen, G. Fiksel, D. Barnak, P.-Y. Chang, R. F. Heeter, A. Link, and D. D. Meyerhofer, "Magnetic collimation of relativistic positrons and electrons from high intensity laser–matter interactions," Physics of Plasmas **21**, 040703 (2014).

[43] J. L. Pebbles, G. Fiksel, M. R. Edwards, J. von der Linden, L. Willingale, D. Mastrosimone, and H. Chen, "Magnetically collimated and focused relativistic charge-neutral electron-positron beams from high powered lasers," , In preparation.

[44] J. Park, N. A. Krall, P. E. Sieck, D. T. Offermann, M. Skillicorn, A. Sanchez, K. Davis, E. Alderson, and G. Lapenta, "High-energy electron confinement in a magnetic cusp configuration," Physical Review X **5** (2015), 10.1103/physrevx.5.021024.